High-performance near-infrared photodetector based on nano-layered MoSe2

doi: 10.1088/1361-6641/aa6819

High-performance Near-Infrared Photodetector Based on Nano-layered $MoSe_2$

Pil Ju Ko[1], Abdelkader Abderrahmane[2], Nam–Hoon Kim[1], and Adarsh Sandhu[3]*

[1] Department of Electrical Engineering, Chosun University, 375, Seosuk–dong, Dong–gu, Gwangju 501–759, Republic of Korea.

[2] Organization for Research Promotion, Research Promotion Center, The University of Electro–Communications (UEC) 1–5–1 Chofugaoka Chofu, Tokyo Japan, 182–8585.

[3] Department of Engineering Science, The University of Electro–Communications (UEC) 1–5–1 Chofugaoka Chofu, Tokyo Japan, 182–8585.

**Corresponding author. E-mail: abderrahmane@uec.ac.jp*

Telephone number: +81-90-4368-1734, Fax number: +81-90-4368-1734

KEYWORDS**:** Two-dimensional materials, transition metal dichalcogenide, molybdenum diselenide, near-infrared photodetector, detectivity.

Abstract

In recent years, the integration of two-dimensional (2D) nanomaterials, especially transition metal chalcogendies (TMCs) and dichalcogendies (TMDCs), into electronic devices have been extensively studied owing to their exceptional physical properties such as high transparency, strong photoluminescence, and tunable bandgap depending on the number of layers. Herein, we report the optoelectronic properties of few-layered $MoSe_2$-based back-gated phototransistor used for photodetection. The photoresponsivity could be easily controlled to reach a maximum value of 238 AW^{-1} under near-infrared light excitation, achieving a high specific detectivity $\left(D^* = 7.6\times10^{11}\ cmHz^{1/2}W^{-1}\right)$. Few-layered $MoSe_2$ exhibited excellent optoelectronic properties as compared with those reported previously for multilayered 2D material-based photodetectors, indicating that our device is one of the best high-performance nanoscale near-infrared photodetector based multilayered two-dimensional materials.

Introduction

Recently, research interest towards low-dimensional material-based near-infrared (NIR) photo-devices have been rapidly increasing owing to their possible wide applications in various fields such as NIR imaging devices, biological sensors, photodetectors, and photovoltaic detectors [1-5]. In particular, layered 2-dimensional (2D) transition metal dichalcogendies (TMDCs) exhibit good optoelectronic performances in a wide range of ultraviolet (UV) to near-infrared (NIR) wavelengths since their bandgap can be controlled by varying the thickness, which can be advantageous for the atomic scale optoelectronic devices [6,7]. Among different transition metal dichalcogendies (TMDCs), molybdenum disulfide (MoS_2) has gained significant research attention owing to its excellent optoelectronic properties, such as high transparency and high photoresponsivity [8]. However, MoS_2 photodetectors can be employed for detecting only in the visible range and their applications in the infrared region are limited [9]. Molybdenum diselenide ($MoSe_2$), another TMDC material, which exhibits an indirect gap of 1.1 eV [10] in the bulk, could be a promising material for near-infrared photodetection applications. In addition, $MoSe_2$ is expected to exhibit enhanced photoresponse properties as compared with MoS_2 owing to their high optical absorption as previously reported by M. Bernardi *et al*. [11].

In this paper, we demonstrate a few-layered $MoSe_2$-based photodetector that can be used in the near-infrared region. The device exhibits a high photoresponsivity of 238 AW^{-1} and an external

quantum efficiency (EQE) of 37,745 % under light excitation with a wavelength of 785 nm. The degradation observed in the optoelectronic properties of the photodetector can be explained based on the trapping effect occurring at the surface and the interface between the active layer and the oxide. Excellent optoelectronic properties are obtained with the values of photoresponsivity, EQE, and specific detectivity exceeding the previously reported values for similar or more complex structures.

Experimental

Titanium electrodes were deposited by electron–beam evaporation on thermally oxidized silicon substrates containing a silicone oxide (SiO_2) layer with a thickness of 300 nm. Few-layered flakes of natural $MoSe_2$ (HQ graphene, Netherlands) was transferred on the Ti electrodes using PDMS (Dow Corning, Toray Co., Ltd) by mechanical exfoliation, and copper electrode was used as the back–gate. The structure was annealed at 400 °C under nitrogen atmosphere for two hours, in the aim to improve the ohmic contacts between titanium electrodes and the nano-layered $MoSe_2$. The optoelectronic properties of the $MoSe_2$ photodetector were measured under laser illumination with a wavelength of 785 nm in atmospheric conditions using a laser power in the range of 0.015–810 µW employing a Semiconductor Characterization System 4200. The thickness was measured using a Pico plus 5500 AFM (Agilent Technologies, USA). NRS–7100 laser Raman spectrometer was used for conducting Raman spectroscopy measurements.

Results and discussion

Thickness dependence on the optical properties of the few-layered $MoSe_2$ was studied. Figure 1(a) shows the optical microscope image of $MoSe_2$ nano-flakes, where areas with different thicknesses are marked as “1 L”, “4 L,” and “B-L”. “1 L” and “4 L” correspond to the flake thickness of 0.7 and 3 nm, respectively, whereas “B-L” is associated to the bulk sample.

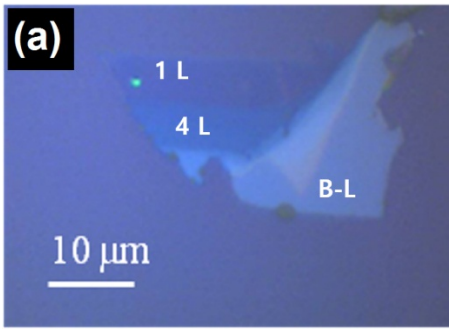

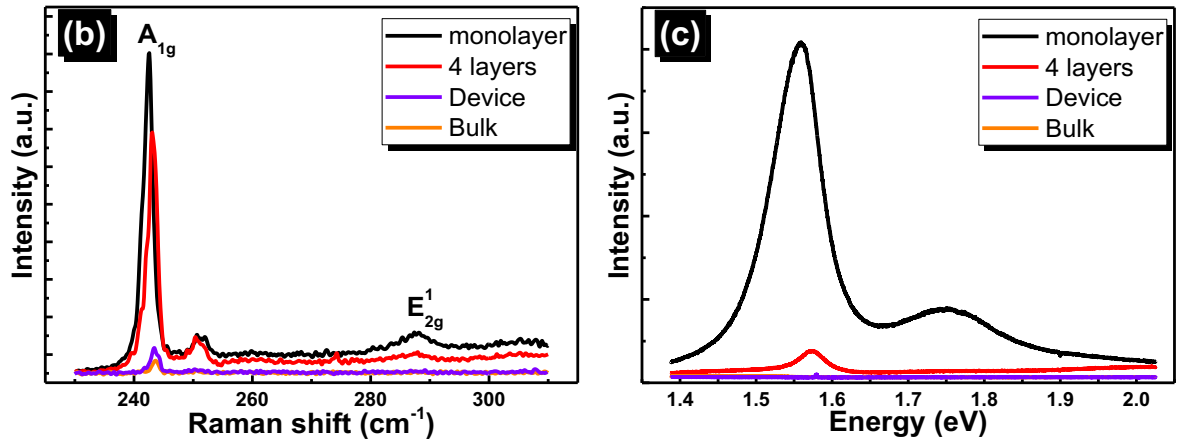

Figure 1 (a) Optical microscope image, (b) Raman spectra, and (c) Photoluminescence (PL) spectra of $MoSe_2$ nano–flakes.

Figure 1 (b) represents the Raman spectra of mono-layered, four-layered, few-layered, and bulk $MoSe_2$, where the few-layered sample that was used in the photodetector shown in Figure 1 (a) is referred to as "Device". Two peaks were observed at around 242 cm^{-1} and 287 cm^{-1}, corresponding to the out-of-plane (A_{1g}) and in-plane (E_{2g}) Raman modes of $MoSe_2$, respectively [12]. A_{1g} peak softens (red-shifted) and the E_{2g} stiffens (blue-shift) with a decrease in the number of layers.

The photoluminescence (PL) spectra of the few-layered $MoSe_2$ are shown in Figure 1(c). $MoSe_2$ exhibits a higher photoluminescence intensity of 1.55 eV in the monolayer form as compared with the sample with more number of layers. However, $MoSe_2$ flake with the thickness of 44 nm (referred to as Device in the figure) exhibits very low photoluminescence intensity. The PL intensity increases with a decrease in the number of layers due to the quantum confinement effect [13].

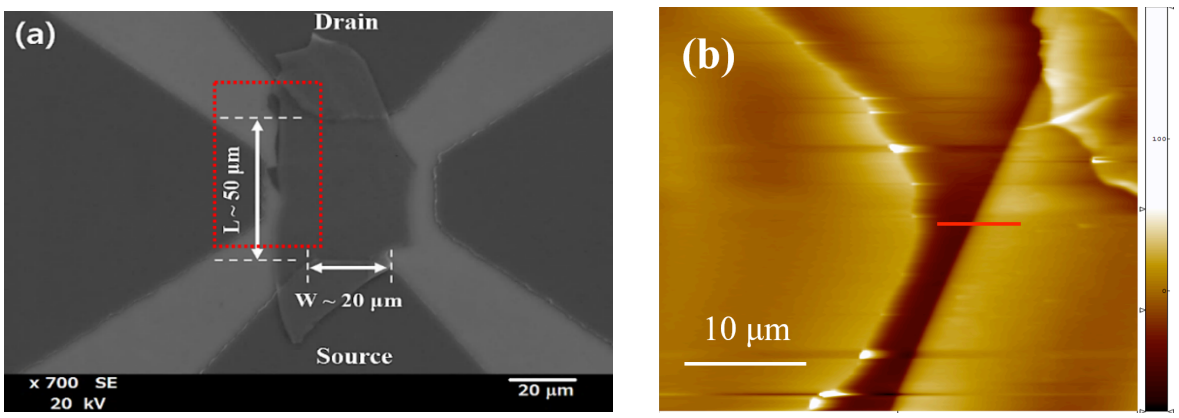

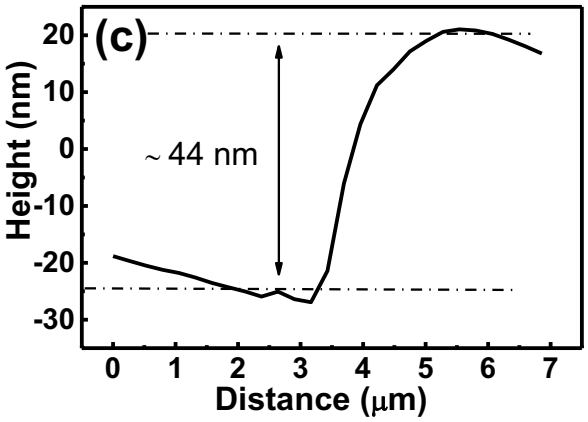

Figure 2 (a) Scanning electron microscopy image of the near-infrared photodetector based on few-layered $MoSe_2$ and (b) AFM image of the NIR photodetector. The red line marks the respective cross section. (c) The flake thickness determined by the topographic analysis.

The scanning electron microscope image of the near-infrared photodetector is shown in Figure 2(a). The device length and width were 50 and 20 μm, respectively. Figure 2(b) represents the AFM image of the device, where the red line indicates the respective cross section. The thickness of the $MoSe_2$ flake was deduced to be 44 nm from the topographic analysis, as seen in Figure 2(c).

Figure 3 shows the transfer curve drain current (I_d or I_{ds}) versus gate voltage (V_G) plot for the phototransistor (shown in the inset of Figure 3) measured under dark and atmospheric conditions.

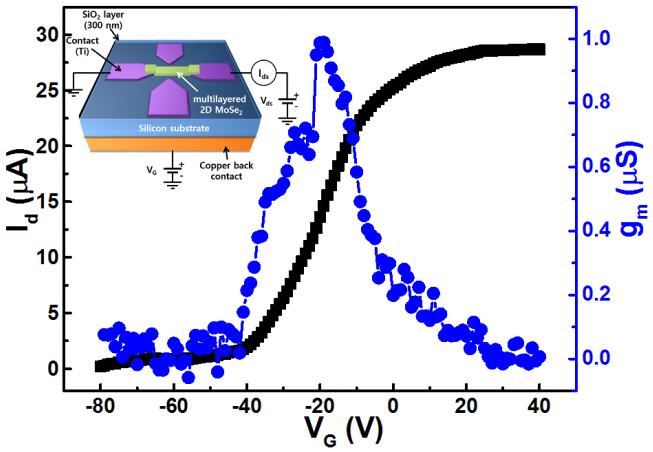

Figure 3 Gate voltage dependence on the drain current and the transconductance of $MoSe_2$ phototransistor at a drain–source voltage of 20 V. Inset: Schematic illustrating the back–gated phototransistor.

The dependence of the drain current on the gate voltage was examined under a polarization voltage (drain–source voltage or V_{ds}) of 20V. The effective mobility (μ_{eff}) was deduced from the drain current – gate voltage transfer function using the equation:

$$\mu_{eff} = [dI_d/dV_g] \times [L/(WC_iV_{ds})] \quad (1)$$

Where L and W are the channel length and width, which are equal to 50 and 20 μm, respectively. C_i is the gate capacitance measured using the equation $C_i = \varepsilon_0\varepsilon_r/d$, where ε_0 and ε_r are the permeability of air and silicon dioxide (SiO_2), respectively. The effective mobility of our device was estimated to be 5.1 $cm^2V^{-1}s^{-1}$ at a polarization voltage of 20 V. The transconductance was measured using the equation:

$$g_m = \left.\frac{dI_d}{dV_G}\right|_{V_d > V_{dsat}} \quad (2)$$

The transconductance is represented by the blue curve in the same figure, indicating a maximum value of 1 μS at a gate voltage of –20 V.

Figure 4 shows the schematic illustration of the energy band diagrams of the $Si/SiO_2/MoSe_2$ contact in the back-gated field effect transistor before and after contact. The work function and the electron affinity of $MoSe_2$ are 5.1 eV [14] and 4.45±0.11 eV [15], respectively. The energy band gap of $MoSe_2$ is about 1.58 eV, as obtained from the photoluminescence results shown in Figure 2(c). As shown in Figure 4, at equilibrium, the phototransistor is in the accumulation mode, where electrons are accumulated at the interface and holes are pushed to the surface. Both electrical characterizations (Figure 3) and Energy band diagram along the vertical axis (Figure 4) showed that the phototransistor works in the accumulation mode, and in the absence of a gate voltage exhibiting a pinch–off voltage of about –40 V.

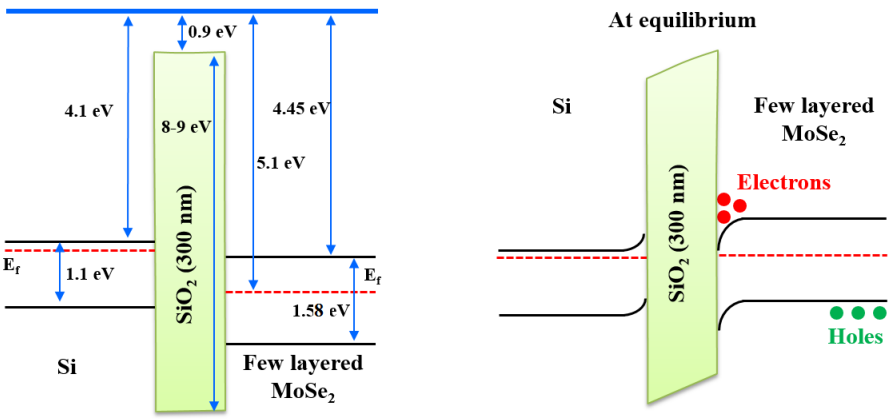

Figure 4 Energy band diagram along the vertical axis illustrating the $Si/SiO_2/MoSe_2$: before contact (Flat-band condition) and after contact (at zero gate voltage).

Figure 5(a) represents the gate voltage dependence on the drain current at different laser power values with a polarization voltage of 20 V. The drain current increases on increasing the laser power due to the increase in the photogenerated carriers. From the linear dependence of the transfer curves illustrated in Figure 5(a), the shift in the threshold voltage can be deduced, which is plotted as a function of the laser power (inset of Figure 5(a)).

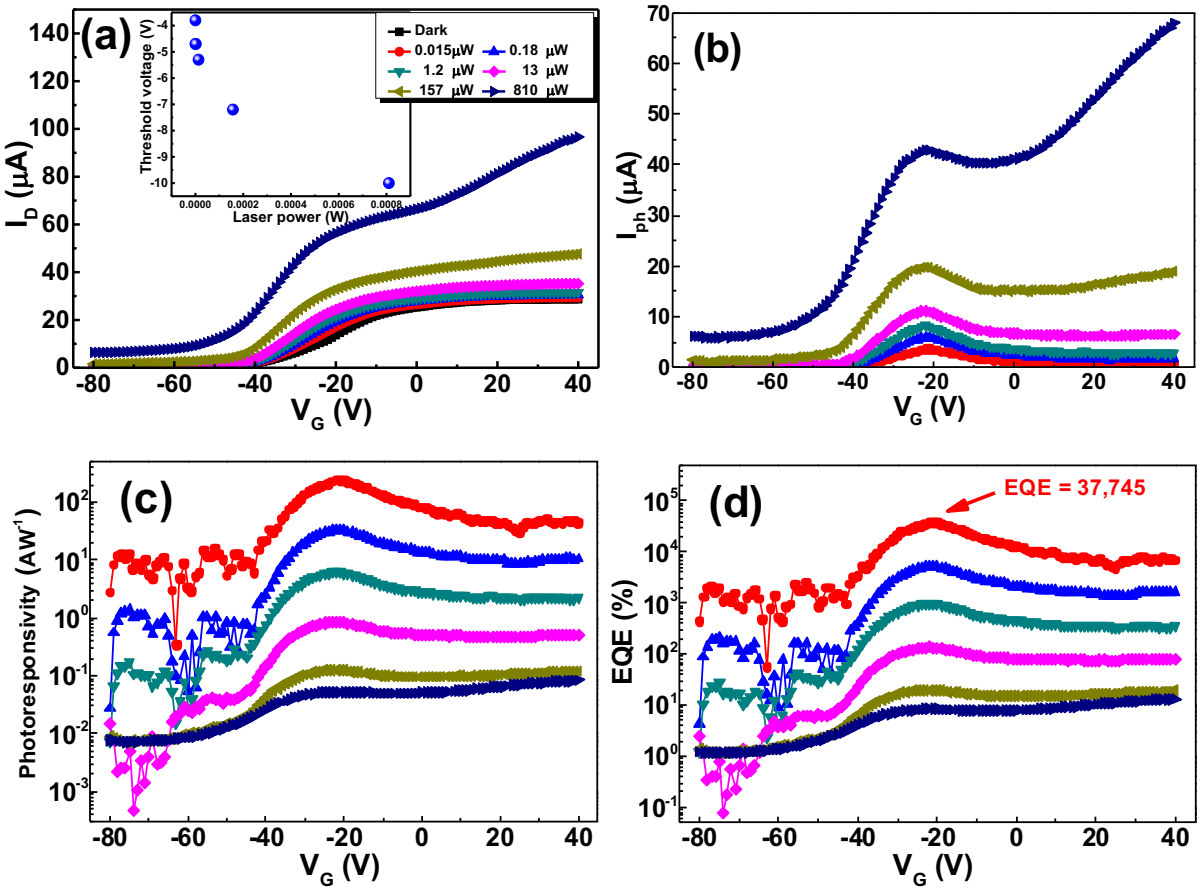

Figure 5 Dependence on the gate voltage at different values of laser power (indicated in (a)) of (a) drain current, (b) photocurrent, (c) photoresponsivity, and (d) EQE of NIR photodetector based on few-layered $MoSe_2$. Inset in (a) shows the laser power dependence on the threshold voltage shift.

The threshold voltage shifts negatively from a value of –41 V in dark conditions to a value of –54 V under illumination with a laser power of 810 μW. The negative shift in the threshold voltage could be attributed to the photogating effect [16].

The photocurrent (I_{ph}) is given by $I_{ph} = I(light) - I(dark)$. I_{ph} increases with an increase in the gate voltage and the laser power, as shown in Figure 5(b). The photoresponsivity (R_λ) can be deduced from the photocurrent using the equation, $R_\lambda = I_{ph}/P$, where P is the laser

power. The photoresponsivity exhibited a high fluctuation in the values at very low gate voltage due to the low subthreshold leakage current, with a maximum value of 238 AW^{-1} obtained at a gate voltage of –22 V, as shown in Figure 5(c). Nevertheless, $MoSe_2$ exhibits a high photoluminescence in the bi- and mono-layer forms, as shown in Figure 2(c). Hence, the photoresponsivity is expected to improve by decreasing the number of layers.

The EQE is measured using the equation, $EQE = hcR_\lambda/e\lambda$, where h is the Planck's constant, e is the elementary electron charge, c is the light velocity, and λ is the excitation wavelength. Figure 5(d) represents the EQE measured at a drain source voltage of 20V at different laser power values. A maximum EQE value of 37,745 % is obtained at a laser power of 0.015 μW and a gate voltage of –22 V. However, EQE decreases with an increase in the laser power since the photoresponsivity decreases. The observed laser power and gate voltage dependence on the photocurrent can be explained using the energy band diagram (Figure 6(a)). At very low gate voltage values (V_G < –22 V), the phototransistor works in the depletion mode as indicated in Figure 6(b) and photons emitted by the laser source generate electron–hole pairs while only electrons can be collected at the drain. Besides, only holes can be collected at the source when the voltage increases (V_G > –22V).

At an optimized gate voltage, barriers at the interface between the electrodes and the multilayered $MoSe_2$ are minimized; therefore, both electrons and holes can be collected at drain and source, respectively, as illustrated in Figure 6(a). This explains the peaks observed in the photocurrent and photoresponsivity curve at a gate voltage of –22 V. However, when the laser power exceeds 157 μW, more electrons are attracted at the interface, when the gate voltage is very high (V_G >> –22 V). Hence, the photocurrent is increased, exhibiting a higher value than that measured at gate voltage of –22 V (Figure 5(b)).

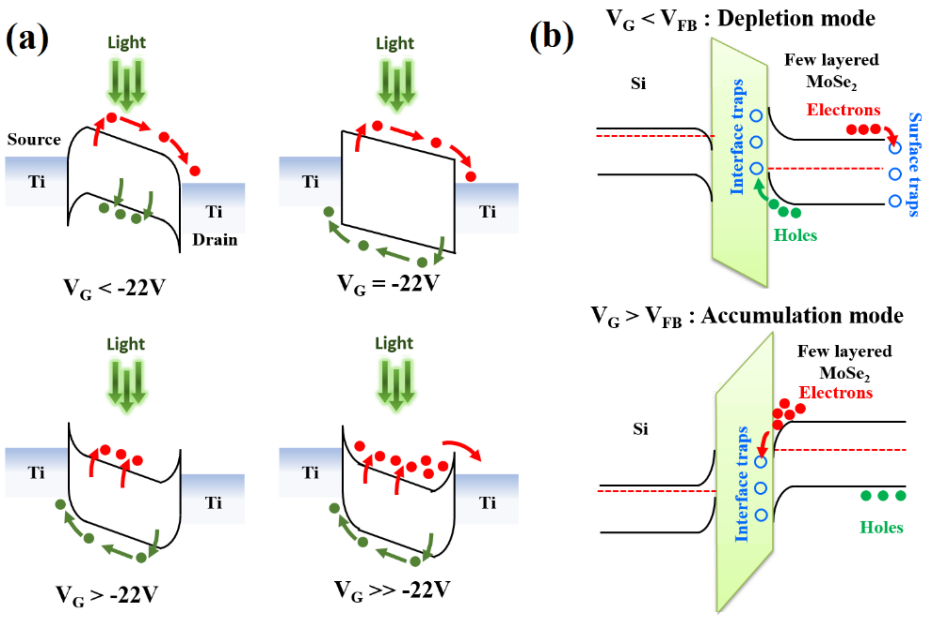

Figure 6 Energy band diagram of $MoSe_2$ multilayer-based phototransistor along (a) the horizontal axis and (b) the vertical axis as a function of gate voltage.

As seen in Figure 7(a), the photocurrent (I_{ph}) exhibits a sublinear dependence on the laser power according to the equation $I_{ph} \propto P^{\alpha}$, where P is the laser power. The exponent α could be deduced to be 0.45, 0.19, 0.30, and 0.36 at the gate voltage of –40, –22, 0, ad 20 V, respectively, in the laser power range of 0.015–157 μW. The sublinear dependence of the photocurrent on the laser power could be associated to the photogating effect [16].

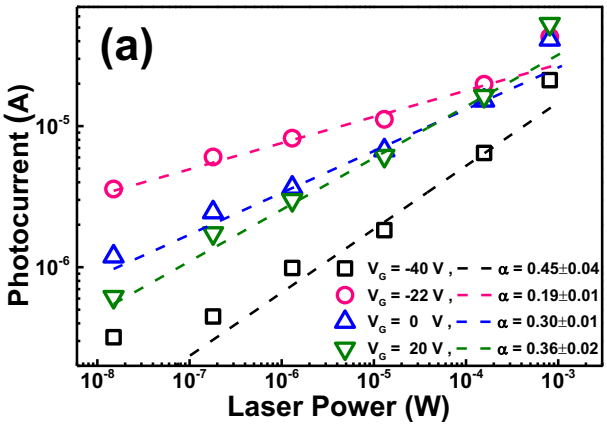

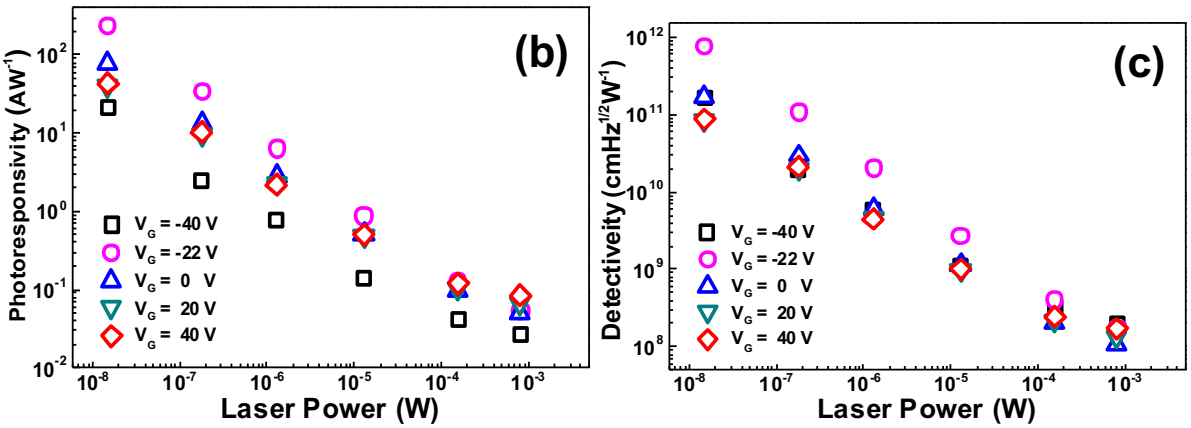

Figure 7 Dependence of (a) photocurrent, (b) photoresponsivity, and (c) detectivity on the laser power at different gate voltage values for the NIR photodetector based on few-layered $MoSe_2$.

The exponent α exhibits minimum values at a gate voltage of –22 V, which can be explained based on the enhanced trapping effect, where both electrons and holes are trapped at the surface and the interface, respectively, as shown in Figure 6(b). In the accumulation mode, only electrons, which are the majority carriers, can be trapped at the interface. The concentration of electrons at the interface is increased with an increase in the gate voltage; therefore, the traps at the interface can be filled and more electrons are available to contribute to the electronic transport. Therefore, the trapping effect is weakened, which explains the increase in the value of α at the positive gate voltage values. When the laser power is increased from 157 μW to 810 μW, α increases to 0.72, 0.47, 0.61, 0.72 and 0.78 for the gate voltage values of –40, –22, 0, 20 and 40, respectively, due to the saturation of the traps with the high concentration of photo–excited electron–hole pairs at high laser power values. Moreover, $MoSe_2$ is expected to exhibit a super linear dependence of the photocurrent at a very high laser power [17]. In addition, the photoresponsivity decreases with an increase in the laser power at different gate voltage values, as seen in Figure 7(b), which confirms the trapping effect at the interface due to the high concentration of traps between SiO_2 and $MoSe_2$ [18], which is measured to be 7.6×10^{12} cm^{-2} by Chamlagain *et al.* [19]. The trapping effect at the surface originates due to the presence of physisorbed gas molecules such as O_2 and H_2O [20].

Another important figure of merit of a photodetector is its smallest detectable signal, referred by the specific detectivity, which is given by the equation $D^* = (AB)^{0.5}R_\lambda,/i_n$ $\left(cm\,Hz^{1/2}\,W^{-1}\right)$, where A is the effective area of the $MoSe_2$ flake in cm^2 (estimated to be 0.38×10^{-4} cm^2), B is the bandwidth, and i_n is the measured noise current [21]. If the shot noise from the dark current is the main noise source, the specific detectivity

can be simplified as $D^* = R_\lambda \times (A)^{0.5}/(2eI_{dark})^{0.5}$, where e is the charge of an elementary electron [22]. The specific detectivity of the NIR photodetector based on $MoSe_2$ as function of laser power and gate voltage is shown in Figure 7(c), indicating a maximum specific detectivity value of 7.6×10^{11} $\left(\mathrm{cmHz^{1/2}W^{-1}}\right)$ at the laser power of 0.015 μW and gate voltage of –22 V. As shown in Table 1, the values for the photoresponsivity and the detectivity obtained for our sample are higher than the corresponding values previously reported for few-layered 2D material-based NIR photodetectors.

Table 1. Comparison of figures-of-merit for NIR photodetectors based on few-layered 2D materials

materials	Spectral range	Responsivity (AW^{-1})	Detectivity ($cmHz^{1/2}W^{-1}$)	Reference
$MoSe_2$	NIR	238	7.6×10^{11}	this work
Black phosphorus	visible–NIR	4.8×10^{-3}	N/A	23
MoS_2	visible–NIR	50–120 ($\times10^{-3}$)	10^{10}–10^{11}	6
Bi_2Se_3	NIR	2.1	1.5×10^{11}	24
WSe_2/MoS_2	NIR	0.3	N/A	25
Graphene/Bi_2Se_3	NIR	7	N/A	26
MoS_2/Black Phosphorus	NIR	0.153	2.13×10^{9}	27

Conclusion

In conclusion, the optoelectronic properties of few-layered $MoSe_2$-based back-gated phototransistor that can be used in the near-infrared region were investigated. The photoresponsivity and the EQE can be controlled to achieve the maximum values of 238 AW^{-1} and 37,745%, respectively, by gate-tuning. A maximum specific detectivity of 7.6×10^{11} $cmHz^{1/2}W^{-1}$ was reported. Our results indicated that few-layered $MoSe_2$-based photodetector is one of the best candidate to be used as high-performance nanoscale near-infrared photodetectors, which might have potential applications in NIR imaging devices, sensors, and photovoltaic detectors.

Acknowledgments

This study was supported by research funds from Chosun University, 2015.

References

[1] Hwang D K, Lee Y T, Lee H S, Lee Y J, Shokouh S H, Kyhm J-H, Lee J, Kim H H, Yoo T-H, Nam S H, Son D I, Ju B-K, Park M-C, Song J D, Choi W K and Im S 2016 Ultrasensitive PbS quantum-dot-sensitized InGaZnO hybrid photoinverter for near-infrared detection and imaging with high photogain NPG Asia Mater. 8 e233

[2] Chou S S, Kaehr B, Kim J, Foley B M, De M, Hopkins P E, Huang J, Brinker C J, Dravid V P 2013 Chemically Exfoliated MoS2 as Near-Infrared Photothermal Agents Angew Chem Int Ed Engl. 52 4160-4164

[3] Luo L-B, Zeng L-H, Xie C, Yu Y-Q, Liang F-X, Wu C-Y, Wang L and Hu J-G 2014 Light trapping and surface plasmon enhanced high-performance NIR photodetector Scientific Reports. 4 3914

[4] Liu Z, Luo T, Liang B, Chen G, Yu G, Xie X, Chen D and Shen G. 2013 High-detectivity InAs nanowire photodetectors with spectral response from ultraviolet to near-infrared Nano Research. 6 (11), 775–783

[5] Luo L–B, Chen J–J, Wang M–Z, Hu H, Wu C–J, Li Q, Wang L, Huang J–A, Liang F–X 2014 Near-Infrared Light Photovoltaic Detector Based on GaAs Nanocone Array/Monolayer Graphene Schottky Junction Adv. Mater. 24, 2794–2800

[6] Choi W, Cho M. Y, Konar, A, Lee J H, Cha G–B, Hong S C, Kim S, Kim J, Jena D, Joo J, Kim S 2012 High-Detectivity Multilayer MoS2 Phototransistors with Spectral Response from Ultraviolet to Infrared Adv Mater. 24, (43), 5832–5836

[7] Jacobs–Gedrim, R B, Shanmugam M, Jain N, Durcan C A, Murphy, M T, Murray, T M, Matyi, R J, Moore R L and Yu B 2014 Extraordinary Photoresponse in Two-Dimensional In2Se3 Nanosheets ACS Nano. 8 (1), 514–521

[8] Zhang Q, Bao W, Gong A, Gong T, Ma D, Wan J, Dai J, Munday J N, He J-H, Hu L and Zhang D 2016 A highly sensitive, highly transparent, gel-gated MoS2 phototransistor on biodegradable nanopaper Nanoscale. 8, 14237–14242

[9] Ye L, Li H, Chen Z and Xu J 2016 Near-Infrared Photodetector Based on MoS2/Black Phosphorus Heterojunction ACS Photonics 3 (4), 692–699

[10] Coehoorn R, Haas C and Groot R A de 1987 Electronic structure of MoSe 2, MoS 2, and WSe 2. II. The nature of the optical band gaps Phys. Rev. B Condens. Matter 35 (12), 6203–6206

[11] Bernardi M, Palummo M and Grossman J C 2013 Extraordinary Sunlight Absorption and One Nanometer Thick Photovoltaics Using Two-Dimensional Monolayer Materials Nano Lett.

13, 3664
[12] Tonndorf P, Schmidt R, Bottger P, Zhang X, Borner J, Liebig A, Albrecht M, Kloc C, Gordan O, Zahn D R T, de Vasconcellos S M and Bratschitsch R 2013 Photoluminescence emission and Raman response of monolayer MoS2, MoSe2, and WSe2 Opt. Express. 21, 4908
[13] Balendhran S, et al. 2013 Two-Dimensional Molybdenum Trioxide and Dichalcogenides Adv. Funct. Mater. 23, 3952–3970
[14] Tsoutsou D, Aretouli K E, Tsipas P, Marquez-Velasco J, Xenogiannopoulou E, Kelaidis N, Aminalragia Giamini S and Dimoulas A 2016 Epitaxial 2D MoSe2 (HfSe2) Semiconductor/2D TaSe2 Metal van der Waals HeterostructuresACS Appl Mater Interfaces 8(3), 1836−1841
[15] Pradhan N R, Rhodes D, Xin Y, Memaran S, Bhaskaran L, Siddiq M, Hill S, M Ajayan P and Balicas L 2014 Ambipolar Molybdenum Diselenide Field-Effect Transistors: Field-Effect and Hall Mobilities ACS nano 8(8), 7923–7929
[16] Island J O, Blanter S I, Buscema M, van der Zant H S J and Castellanos–Gomez A 2015 Gate Controlled Photocurrent Generation Mechanisms in High-Gain In2Se3 Phototransistors Nano letters. 15 (12), 7853
[17] Klee V, Preciado E, Barroso D, Nguyen A E, Lee C, Erickson K J, Triplett M, Davis B, Lu I H, Bobek S, McKinley J 2015 Superlinear Composition-Dependent Photocurrent in CVD-Grown Monolayer MoS2(1–x)Se2x Alloy Devices Nano letters. 15 (4), 2612–2619
[18] Abderrahmane A, Ko P J, Thu T V, Ishizawa S, Takamura T and Sandhu A 2014 High photosensitivity few-layered MoSe2 back-gated field-effect phototransistors Nanotechnology. 25, 365202
[19] Chamlagain B, Li Q, Ghimire N J, Chuang H-J, Perera M M, Tu H, Xu Y, Pan M, Xaio D, Yan J, Mandrus D and Zhou Z 2014 Mobility Improvement and Temperature Dependence in MoSe2 Field-Effect Transistors on Parylene-C Substrate ACS Nano. 8 (5), 5079–5088
[20] Tongay S, Zhou J, Ataca C, Liu J, Kang J S, Matthews T S, You L, Li J, Grossman J C and Wu J 2013 Broad-Range Modulation of Light Emission in Two-Dimensional Semiconductors by Molecular Physisorption Gating Nano letters. 13(6), 2831–2836
[21] Zhang W, Huang J-K, Chen C-H, Chang Y-H, Cheng Y-J and Li L-J 2013 High-Gain Phototransistors Based on a CVD MoS 2 Monolayer Adv. Mater. 25 (25), 3456
[22] Liu X, Gu L, Zhang Q, Wu J, Long Y and Fan Z 2014 All-printable band-edge modulated ZnO nanowire photodetectors with ultra-high detectivity Nat. Commun. 5, 4007
[23] Buscema M, Groenendijk D J, Blanter S I, Steele G A, van der Zant S H J and Castellanos–Gomez A 2014 Fast and Broadband Photoresponse of Few-Layer Black Phosphorus Field-

Effect Transistors Nano Lett. 14, 3347−3352
[24] Chen G, Yu Y, Zheng K, Ding T, Wang W, Jiang Y, Yang Q 2015 Fabrication of Ultrathin Bi2S3 Nanosheets for High-Performance, Flexible, Visible–NIR Photodetectors Small. 11, 2848–2855
[25] Park M J, Min J K, Yi S–G, Kim J H, Oh J and Yoo K-H 2015 Near-infrared photodetectors utilizing MoS2-based heterojunctions J. Appl. Physics. 118, 044504
[26] Kim J, Jang H, Koirala N, Sim S, Lee J-B, Kim U J, Lee H et al 2016 Gate-tunable, high-responsivity, and room-temperature infrared photodetectors based on a graphene-Bi2Se3 heterostructure In CLEO: Science and Innovations. SF2E–3
[27] Ye L, Li H, Chen Z and Xu J 2016 Near-Infrared Photodetector Based on MoS2/Black Phosphorus Heterojunction ACS Photonics. 3, 692–699